AD-A140 076 FINAL SCIENTIFIC REPORT FOR ONR CONTRACT N00014-76-C-0182(U) ARIZONA UNIV TUCSON JAN 83 N00014-76-C-0182

1/1

UNCLASSIFIED

F/G 20/4 NL

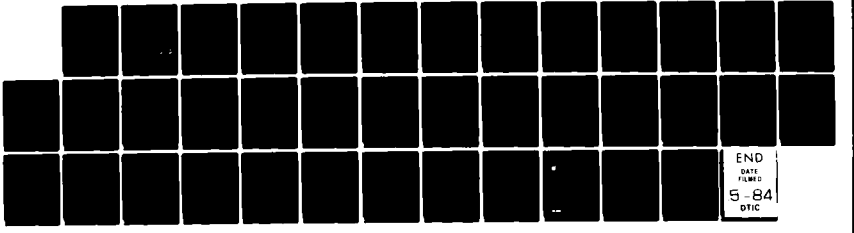

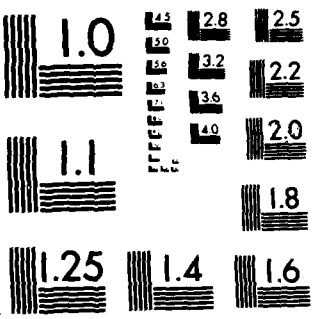

(1)

FINAL SCIENTIFIC REPORT

FOR

ONR Contract No. N00014-76-C-0182

Principal Investigator: Dr. K.-Y. Fung

University of [redacted]

Tucson, Arizona

FINAL SCIENTIFIC REPORT

ONR Contract No. N00014-76-C-0182

Introduction

This final report summarizes our research activities on ONR Contract No. N00014-76-C-0182 from February, 1976 to January, 1983. These research activities resulted in twenty four publications and twenty two oral presentations, were in part supported by the NASA and the AFOSR.

Fictitious Gas Design Method

The design technique of using fictitious gas to achieve shock free transonic flight conditions had been studied and extended to the design of wings, airfoils, and supersonic conical bodies. Its practicality and the ability of obtaining near optimal designs have been summarized in the review paper presented at the International Congress of Aeronautical Sciences Meeting, Seattle, Washington.

The new application to the design of supersonic conical bodies was reported in Dr. Sritharan's dissertation and also mentioned in the ICAS paper. Only the example of a circular cone at an angle of incident was given. Hopefully, Dr. Sritharan will be able to complete this study at ICAS where he is a post-doctoral fellow. A general conclusion of this study at this stage is that the applicability of the fictitious method in conical flows is more limited than in plane transonic flow.

Conical Flows

A fully conservative finite area code based on the potential

approximation for conical flows has been developed in Dr. Sritharan's dissertation. This work, being the first using finite area approach and one that generalizes Jameson's iteration procedure to general curvilinear systems, was presented at the AIAA Fluid, Plasmadynamics and Heat Transfer Conference, St. Louis, Missouri June, 1982. An application of this code is to design conical bodies at incident with shock free cross flow, mentioned above.

Unsteady Transonic Flow Computations with Input Pressure Distributions

Derived from our earlier belief that an accurate steady pressure distribution with correct shock strength and location is important for the prediction of unsteady transonic responses, an inverse algorithm IAF2, accepting pressure distributions instead of airfoil coordinates, is developed to provide the steady flow fields needed in unsteady computations. This algorithm has been integrated into our version of LTRAN and the time linearized code UTFC developed in our earlier studies. This work was presented at the AIAA Fluid, Plasmadynamics and Heat Transfer Conference. Very good agreement compared with experimental results in predicting phase lags and magnitudes of unsteady responses for attached transonic flows is obtained using this procedure.

Unsteady Wind Tunnel Interference

Alerted by previous research on the proper far-field boundary conditions for unsteady transonic flow, we have concluded in a study, as part of Mr. Przybytkowski's dissertation, that two dimensional wall interferences are most critical in the low to moderate reduced frequency range; that resonance conditions can be predicted using linear acoustic theory, with slight modifications due to nonlinear effects, and that part of the discrepancies between experimental measurement

and numerical calculations may be attributed to the uncertainities in wall conditions. A review of this work will appear in a book entitled, "Recent Advances in Numerical Methods in Fluids, Vol. IV," edited by Habashi. A copy of this review paper is in Appendix C.

Inviscid Flows with Shock Induced Vorticity

In order to compute the flow after a moderately strong shock accurately, we have studied and confirmed the logartithmic nature of the local solution near the shock root and found that the vorticity induced by the curvature of the shock, despite the well known singularity at the root, is finite and given by a formula in terms of the upstream Mach number, density and the curvature of the body at the shock root. A technical note on this result is published in the AIAA Journal attached as Appendix D.

Conclusion

During the course of this research, we have completed various studies in transonic flow, resulting in publications, three doctoral dissertations and two master reports, and seven presentations. These results reflect not only this support, but also AFOSR support. We conclude this report with a list of publications from January, 1977 through June, 1983.

APPENDIX A

APPENDIX A

Papers, Reports 1977-1983

** 1. Fung, K.-Y., "Vorticity at the Shock Foot in Inviscid Flow," AIAA Journal, Vol. 21, No. 6, pp. 915-916, June, 1983.

** 2. Fung, K.-Y., Sobieczky, H. and Seebass, A.R., "Shock-Free Airfoil, Wing and Turbojet Blade Design," ICAS/AIAA Aircraft Systems & Technology Conference, Seattle, Washington, Preprint ICAS-82-3.7.1, 1982.

** 3. Fung, K.-Y. and Chung, A., "Computation of Unsteady Transonic Aerodynamic Responses Using a Prescribed Input Steady State Pressure Distribution," AIAA/ASME 3rd Joint Thermophysics, Fluids, Plasma and Heat Transfer Conference, Paper 82-0956, St. Louis, Missouri, 7-11 June, 1982. (to appear in AIAA Journal)

** 4. Sritharan, S.S. and Seebass, A.R., "A Finite Area Method for Nonlinear Conical Flows," AIAA/ASME 3rd Joint Thermophysics, Fluids, Plasma and Heat Transfer Conference, Paper 82-0995, St. Louis, Missouri, 7-11 June, 1982.

** 5. Fung, K.-Y., "A Model for Unsteady Transonic Indicial Responses," AIAA Journal, Technical Note 82-4188.

*** 6. Seebass, A.R., "Shock-Free Configurations in Two- and Three Dimensional Transonic Flow," MRC Symposium on Transonic, Shock and Multi-dimensional Flows," Advances in Scientific Computing, Academic Press, 1982.

** 7. Seebass, A.R. and Fung, K.-Y., "Unsteady Transonic Flows: Time-Linearized Calculations," Numerical and Physical Aspects of Aerodynamic Flows, Springer-Verlag, T. Cebeci, editor, 1982.

** 8. Fung, K.-Y., Seebass, A.R. and Dickson, L.J., "An Effective Algorithm for Shock-Free Wing Design," AIAA Paper No. 81-1236.

** 9. Hassan, A. and Seebass, A.R., "Transonic Airfoils with a Given Pressure Distribution," AIAA Preprint No. 81-1235.

** 10. Fung, K.-Y., "Far-Field Boundary Conditions for Unsteady Transonic Flows," AIAA Journal, Vol. 19, No. 2, pp. 180-183, 1981.

* 11. Fung, K.-Y., "Shock Wave Formulation at a Caustic," SIAM J. Appl. Math., Vol. 39, No. 2, pp. 355-371, October, 1980.

** 12. Fung, K.-Y., Sobieczky, H. and Seebass, R., "Shock-Free Wing Design," AIAA Journal, Vol. 13, No. 10, pp. 1153-1158, October, 1980.

13. Sobieczky, H. and Seebass, A.R., "Adaptive Airfoils and Wings for Efficient Transonic Flight," ICAS Preprint, Munich, October, 1980.

** 14. Nebeck, H., Seebass, A.R. and Sobieczky, H., "Inviscid-Viscous Interactions in the Nearly Direct Design of Shock-Free Supercritical Airfoils," AGARD Fluid Dynamics Panel Symposium Computation of Viscous-Inviscid Interactions, Colorado Springs, September, 1980.

* 15. Moran, J., Cole, K. and Wahl, D., "Analysis of Two-Dimensional Incompressible Flows by a Subsurface Panel Method," AIAA Journal, Vol. 18, No. 5, pp. 526-533, May, 1980.

** 16. Tijdeman, H. and Seebass, R., "Transonic Flow Past Oscillating Airfoils," Ann. Rev. Fluid Mech., 12, pp. 181-222, 1980.

**** 17. Cramer, M.S., "Lifting Three-Dimensional Wings in Transonic Flow," J. Fluid Mech., Vol. 95, Part 2, pp. 223-240, 1979.

*** 18. Sobieczky, H, Yu, N.J., Fung, K.-Y. and Seebass, A.R., "A New Method for Designing Shock-Free Transonic Configurations," AIAA Journal, Vol. 17, No. 7, pp. 722-729, July, 1979.

** 19. Sobieczky, H., "Related Analytical Analog and Numerical Methods in Transonic Airfoil Design," AIAA 12th Fluid & Plasma Dynamics Conference, Paper 79-1556, Williamsburg, Virginia, 23-25 July, 1979.

*** 20. Seebass, A.R., Yu, N.J. and Fung, K.-Y., "Unsteady Transonic Flow Computations," AGARD Conference on Unsteady Aerodynamics, CP No. 227, pp. 11, 1-17, 1978.

** 21. Fung, K.-Y., Yu, N.J. and Seebass, R., "Small Unsteady Perturbations in Transonic Flows," AIAA Journal, Vol. 16, No. 8, pp. 815-822, August, 1978.

** 22. Cramer, M.S. and Seebass, A.R., "Focusing of Weak Shock Waves at an Arete," J. Fluid Mech., Vol. 88, Part 2, pp. 209-222, 1978.

**** 23. Yu, N.J., Seebass, A.R. and Ballhaus, W.F., "Implicit Shock-Fitting Scheme for Unsteady Transonic Flow Computations," AIAA Journal, Vol. 16, No. 7, pp. 673-678, July, 1978.

Doctoral Dissertation and Master Reports

Hassan, A., "Transonic Airfoils with a Given Pressure Distribution," Ph.D. Thesis, University of Arizona, Aerospace & Mechanical Engineering, 1981.

Chung, Wei-hsin, "Computational Studies of Unsteady Transonic Aerodynamic Responses Using Prescribed Input Steady Pressure," Masters Report, University of Arizona, Aerospace & Mechanical Engineering, 1982.

Sritharan, S.S., "Nonlinear Aerodynamics of Conical Delta Wings," Ph. D. Thesis, University of Arizona, Aerospace & Mechanical Engineering, 1982.

Przybytkowski, S.M., "Effects of Wall Interference on Unsteady Transonic Flows," Ph.D. Thesis, University of Arizona, Applied Mathematics, 1983.

Nebeck, H., "Three Dimensional Grids for Aerodynamic Applications," Masters Report, University of Arizona, Aerospace & Mechanical Engineering, 1983.

APPENDIX B

APPENDIX B

Talks 1977-1983

University of Arizona, Aerospace and Mechanical Engineering Seminar, February, 1982. (Fung)

AIAA/ASME 3rd Joint Thermophysics, Fluids, Plasma and Heat Transfer Conference, St. Louis, Missouri, June, 1982. (Two talks- Fung, Sritharan)

13th Congress of the International Council of the Aeronautical Sciences, Seattle, Washington, August, 1982. (Fung)

DFVLR, Gottingen Colloquium, May, 1981. (Fung)

MRC Symposium of Transonic, Shock, and Multi-dimensional Flows, May, 1981. (Seebass)

AIAA 14th Fluid and Plasma Dynamics Conference, June, 1981. (Two talks- Hassan, Seebass)

7th Annual General Aviation Technologyfest, Wichita, November, 1980. (Seebass)

International Council of the Aeronautical Sciences Meeting, Munich, October, 1980. (Sobieczky)

AGARD Fluid Dynamics Panel Symposium on Viscous-Inviscid Interactions, Colorado Springs, September, 1980. (Seebass)

University of Haifa Colloquium, May, 1980. (Seebass)

University of Tel Aviv Mathematics Seminar and Fluid Mechanics Colloquium, May, 1980. (Seebass)

Israel Avaiation Industry, Tel Aviv, May, 1980. (Seebass)

DFVLR, Gottingen Colloquia (3), May, 1980. (Seebass)

University of Minnesota Colloquium, Minneapolis, April, 1980. (Seebass)

University of Colorado Colloquium, Boulder, April, 1980. (Seebass)

California Institute of Technology Colloquium, Pasadena, April, 1980. (Seebass)

Unsteady Transonic Flow, NASA Langley Workshop, February, 1980. (Seebass)

Shock-Free Flows, NASA Lewis, November, 1979. (Seebass)

AIAA 12th Fluid and Plasma Dynamics Conference, Williamsburg, July, 1979. (Two talks- Fung, Sobieczky)

Lockheed-Georgia Company Seminar, July, 1979. (Seebass)

ADDSL/AFOSR Review, Dayton, June, 1979. (Seebass)

Lockheed-California Company Seminar, April, 1979. (Seebass)

APPENDIX C

A SIMPLE, ACCURATE AND EFFICIENT ALGORITHM FOR UNSTEADY TRANSONIC FLOW

K.-Y. Fung

Aerospace and Mechanical Engineering
University of Arizona
Tucson, Arizona

1. INTRODUCTION

This chapter describes an algorithm for computing an airfoil's response to small unsteady perturbations. The development of the algorithm is sufficiently detailed for the experienced reader to code. The algorithm is simple, efficient, and incorporates several special features that make it an effective method of determining the aerodynamic response of airfoils and, using strip theory, wings with modest sweepback. The special features include an accurate modeling of the far-field boundary condition, the ability to prescribe the airfoil's steady-state pressure distribution and determine the small perturbation steady-state flow field consistent with this prescription, and the capability of generating results for low reduced frequencies through the superposition of the results for a single step change, that is, an indicial motion.

We begin with a brief discussion of the importance of these flows, then state the governing equations and discuss their time linearization. Special care is taken to describe the treatment of moving shock waves. The equations and boundary conditions are then discretized using the usual ADI scheme. The far-field for a potential vortex with wake is used to provide the appropriate far-field boundary condition. The procedure for finding the airfoil that corresponds to a given prescribed pressure distribution is then described. The advantages of using an indicial response are then discussed. Some numerical examples and a discussion of the effects of wind tunnel walls on unsteady transonic testing follow. Concluding remarks summarize the capabilties of the algorithm described.

2. GOVERNING EQUATIONS

In most aeroelastic problems, structural deformations are assumed to be small and, hopefully, will remain small through aerodynamic and structural damping. However, oscillatory modes of a wing and its control surfaces may extract energy from free stream and grow until the structure disintegrates. Flight boundaries that prevent aircraft from operating at or near such conditions are established in aircraft flight tests. An essential element in aircraft design is the prediction of such flutter boundaries. To establish these boundaries, it is fair to assume that the unsteady aerodynamic disturbances to the already established steady flow field about the aircraft are small. This is generally true, except in transonic flow where the unsteady pressure fluctuations may be large due to shock motions. Nevertheless, it is possible to correctly account for this shock motion by linearizing about the steady-state flow. Care must be taken to accurately capture any shock waves in the steady-state flow.

We confine our study to thin airfoils with a thickness-to-chord ratio τ of the order $(1-M_\infty^2)^{3/2}$. Then the governing equation for the perturbation velocity potential ϕ in two space dimensions is

$$-k^2M_\infty^2\phi_{tt}-2kM_\infty^2\phi_{xt}+[1-M_\infty^2-(\gamma+1)M_\infty^2\phi_x]\phi_{xx}+\phi_{yy} = 0, \qquad (1)$$

where M_∞ is the free stream Mach number, γ is the ratio of specific heats, and k is the reduced frequency obtained from the circular frequency nondimensionalized by the free stream velocity U divided by the airfoil chord c. This equation, first derived by Lin et al. [1], can be obtained from a systematic expansion of the continuity and the Bernoulli equations in the thickness ratio τ. It is valid for inviscid and irrotational flow, which implies an attached boundary layer, and the potential approximation requires that any shock wave be weak. For $k = O(1)$ the nonlinear term is inconsequential and may be dropped.

The boundary condition on the airfoil is the linearized flow tangency condition, i.e.,

$$\phi_y(x,0^{\pm},t) = \tau\left[Y^o_x + \frac{\varepsilon}{\tau}\,(Y^u_x + kY^u_t)\right], \quad 0 \le x \le 1, \qquad (2)$$

where there are separate functions $Y(x, t)$ for the upper and lower surface. Here the airfoil shape has been decomposed into a fixed part, τY^o, and a moving part, $\varepsilon Y^u(x,t)$, of amplitude ε. In the wake behind the trailing edge, the pressure coefficient, c_p, is continuous and we require

$$\left[\!\left[\ \phi_x + k\phi_t\ \right]\!\right] = 0, \text{ across } y = 0 \text{ for } x > 1; \qquad (3)$$

here $\left[\!\left[\ "\ \right]\!\right]$ denotes jump of the bracketed quantities. At large distances, all steady disturbances should decay properly and all unsteady disturbances allowed to radiate to infinity. We shall discuss the implementation of these conditions later.

2.1 Far-Field Boundary Conditions

At large distances all disturbances must decay. However, the size of the computational domain necessary for trivial boundary conditions has a profound effect on the efficiency of an algorithm. A typical acoustic wave of frequency ω has a wave length a/ω or (c/kM_∞), and thus requires a mesh no bigger than the chord c to resolve this wave for the range of k considered here. In unsteady transonic flow, the characteristic time scale for an unsteady process to reach a new equilibrium point is typically the time required for the airfoil to travel several hundred chord lengths. A satisfactory grid needs to be 100 chord lengths in size to prevent outgoing waves from reflecting off the grid and requires about 150 intervals with approximately 50 of these clustered near the airfoil to resolve the flow details. The large size insures that waves reflected from any numerical boundary will not have sufficient time to return to the airfoil and contaminate the results.

Far away, a change of incidence of the airfoil behaves like a potential vortex that introduces a jump in potential, $\Delta\Gamma$, at the origin at time t_o. Later, the disturbances caused by this change propagate in time and in space, following the characteristic $t + x - (x^2 + y^2)^{1/2}$. An exact solution of the linear perturbation potential can be found using analytical techniques [2]. In two dimensions this result is

$$\Delta\phi = \frac{\Delta\Gamma(t_o)}{2\pi}\, f\left(x, \beta y, \frac{\beta^2}{kM_\infty^2}(t-t_o)\right)$$

where

$$f(x,y,t) = H(t+x-(x^2+y^2)^{1/2}) \cdot$$

$$\left\{\tan^{-1}\frac{[(t^2+2xt-y^2)^{1/2} + t]}{y} + \tan^{-1}\frac{[(t^2+2xt-y^2)^{1/2} - t]}{y}\right\},$$

$\beta = (1-M_\infty^2)^{1/2}$, and,

$$H(t') = \begin{cases} 0 & t' < 0 \\ 1 & t' > 0 \end{cases} .$$

A similar result can be found in three dimensions.

For arbitrary changes in circulation, $\Gamma(t)$, a superposition of this result gives the general two-dimensional far field, namely,

$$\phi(x,y,t) = \frac{1}{2} \int_0^t f(x,\beta y, \frac{\beta^2}{kM_\infty^2}(t-t_o)) \frac{d\Gamma(t_o)}{dt_o} dt_o \qquad (4)$$

For a given circulation history $\Gamma(t)$, which must be kept, Equation (4) can be evaluated very efficiently for each point of the far-field boundary. Using the result (4), a satisfactory computational domain can be as small as 15 chords, providing nearly a factor of 10 savings in the storage requirements and execution time.

2.2 Time-Linearization of the Governing Equations

An effective way to solve Equation (1) is to first obtain the steady-state solution, say $\phi^o(x, y)$, satisfying the steady boundary condition,

$$\phi_y^o(x, 0) = \tau Y_x^o, \quad 0 \leq x \leq 1,$$

and then compute ϕ, which will deviate only slightly from ϕ^o for small unsteady disturbances, i.e., $|\phi - \phi^o| = O(\varepsilon)$, except in the regions of shock motion. This suggests the introduction of an unsteady potential $\psi(x, y, t)$ defined by

$$\phi(x, y, t) = \phi^o(x, y) + \varepsilon\psi(x, y, t).$$

Substituting this identity into Equation (1) and neglecting terms $O(\varepsilon^2)$, one obtains the time-linearized equation for unsteady small disturbances:

$$-k^2M_\infty^2\psi_{tt} - 2kM_\infty^2\psi_{xt} + \{[1-M_\infty^2 - (\gamma+1)M_\infty^2\phi_x^o]\psi_x\}_x + \psi_{yy} = 0. \qquad (5)$$

The corresponding boundary conditions are

$$\psi_y(x, 0, t) = Y_x^u + kY_t^u, \quad 0 \leq x \leq 1; \qquad (6a)$$

$$[\![\psi_x + k\psi_t]\!] = 0, \quad 1 < x \qquad (6b)$$

It should be noted that in cases where the shock excursions are large, this linearization is no longer possible. The coefficient, $[1-M_\infty^2 - (\gamma+1)M_\infty^2\phi_x^o]$, in Equation (5) obtained from the steady state determines where the flow is subsonic or supersonic. As a shock moves, the region ahead must be supersonic and the region behind, subsonic in our approximation, and this implies that the spatial properties must change accordingly. Unless the region where the shock travels is small, Equation (5) is inadequate and Equation (1) should be used instead.

However, using Equation (5), once the steady state is determined from computations or experimental measurements, the geometry of the airfoil as well as ϕ_y can be ignored completely and grid refinements usually associated with a complex geometry are no longer needed.

Equations (1) and (5) can be further simplified by dropping the k^2 terms; as we noted earlier for $k = O(1)$, the nonlinear term is inconsequential. Thus, we are primarily interested in low-to-moderate frequency motions and these are the most likely to lead to flutter. Indeed, the appropriate singular limit is $k = O(\tau^{2/3})$. Thus the appropriate equations for low frequencies are

$$-2kM_\infty^2\phi_{xt} + [1-M_\infty^2 - (\gamma+1)M_\infty^2\phi_x]\phi_{yy} + \phi_{yy} = 0, \qquad (7a)$$

in place of Equation (1), and

$$-2kM_\infty^2\psi_{xt} + \{[1-M_\infty^2 - (\gamma+1)M_\infty^2\phi_x^0]\psi_x\}_x + \psi_{xy} = 0, \qquad (7b)$$

in place of Equation (5).

2.3 Unsteady Shock Jump Relations

Equation (7a) admits discontinuous solutions, that is shocks, satisfying the condition derived from its conservative form, namely,

$$-2kM_\infty^2[\![\phi_x]\!]\frac{dx_s}{dt} - [1-M_\infty^2-(\gamma+1)M_\infty^2\tilde{\phi}_x][\![\phi_x]\!] + [\![\phi_y]\!] = 0, \qquad (8)$$

together with the condition derived from irrotational assumption

$$\left(\frac{dy}{dx}\right)_s = -\frac{[\![\phi_x]\!]}{[\![\phi_y]\!]}. \qquad (9)$$

Equation (8) states that the shock excursion, $x_s(y, t)$, can be integrated forward in time knowing the jump in ϕ_x and ϕ_y, and the mean value, $\tilde{\phi}_x$, across the discontinuity. Equation (9) describes the shape of this discontinuity at any instant in time.

For thin airfoils at transonic Mach numbers, the shock waves that occur are nearly normal to the free stream, therefore the jump in ϕ_y in Equation (8) can be neglected, resulting in the simplified equation for the motion of normal shocks,

$$\frac{dx_s}{dt} = \frac{\gamma+1}{2k}\left\{\frac{M_\infty^2-1}{(\gamma+1)M_\infty^2} + \tilde{\phi}_x\right\} \tag{10}$$

Note however, that the speed of the shock depends on $\tilde{\phi}_x$ and will vary with y. To be consistent with the normal shock assumption, shock motion must be uniform in y at all times. Thus, Equation (8) is only integrated at one y location, $y = y^o$, for each shock $x_s(t)$. The validity of this approximation stems from the observation that the shock curvature away from the shock foot where it is singular is the same order as the airfoil curvature and hence $O(\tau/c)$ and consequently small. A careful comparison of the results found involving this approximation with results obtained without it, (Yu et al. [3]), confirmed this observation, as did Fung and Chung [4].

Because our changes to the steady flow field are $O(\varepsilon)$, it is clear that the shock motion must remain small. If we linearize the shock position about its steady-state value x_s^o,

$$x_s(t) = x_s^o + \delta x(t),$$

then we find

$$\delta\frac{dx}{dt} = \frac{(\gamma+1)\varepsilon}{2k}\tilde{\psi}_x(x_s^o, t) \tag{11}$$

and we note that for the reduced frequencies of principal concern, namely $k = O(\tau^{2/3})$, we must have

$$\delta \sim \left(\frac{\varepsilon}{\tau^{2/3}}\right) = o(1),$$

which defines the amplitudes of the unsteady motion for which time linearization is valid. Thus, for $k = O(\tau^{2/3})$ and with $\varepsilon\tau^{-2/3} = o(1)$, we may use the time-linearized result (7b).

Near the region where shock motions occur, perturbations are no longer small. The derivatives of ϕ can change sign abruptly depending on whether the shock is on the upstream or downstream side. This would invalidate our small disturbance assumption unless ψ is treated differently to account for large disturbances due to shock motions. Consider derivatives of the potential function ϕ at time $t = 0$. The potential ϕ will have a discontinuous slope at x_s^o as shown in Figure 1.

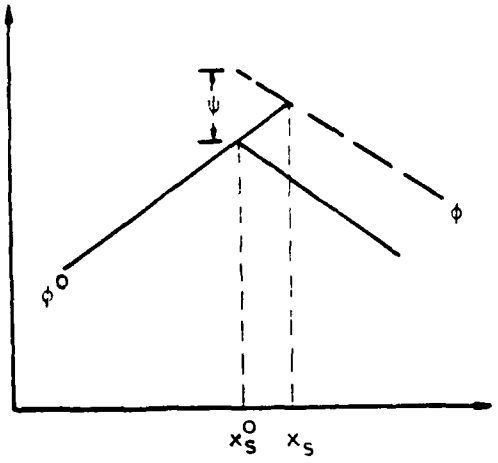

Figure 1. A sketch of ϕ^o and ϕ in the vicinity of the unperturbed shock.

Let us assume that this discontinuity moves to a new location x_s at a late time t due to downstream disturbances. To account for this change, let ϕ be expanded about the point x_s^o:

$$\phi(x,t) = \phi(x_s^o,t) + \phi_x(x_s^o,t)(x-x_s^o) + O(x-x_s^o)^2.$$

If $\phi(x_s^o,t)$ is replaced by $\varphi^o(x_s^o) + \varepsilon\psi(x_s^o,t)$, and we require that ϕ be continuous at the new shock point x_s, then there must be no jump in ϕ at that point. Thus,

$$\left[\!\left[\phi(x_s,t)\right]\!\right] = 0 = \left[\!\left[\phi^o(x_s^o)\right]\!\right] + \varepsilon\left[\!\left[\psi(x_s^o,t)\right]\!\right] + \left[\!\left[\phi_x{}^o(x_s^o)\right]\!\right](x_s-x_s^o) + O[\varepsilon(x_s-x_s^o)] + O(x_s-x_s^o)^2 + \ldots.$$

Now, since both $x_s-x_s^o$ and ε are small, the change of potential at the old location due to shock motion is to the lowest order,

$$\varepsilon\left[\!\left[\psi\right]\!\right] = -\left[\!\left[\phi_x^o\right]\!\right](x_s-x_s^o),$$

which is proportional to the jump of ϕ_x^o at the old location and to the shock excursion $(x_s-x_s^o)$. To accomplish this shock motion, we analytically (i.e., linearly) continue ψ upstream to the steady-state shock position where we have introduced a discontinuity in ψ. Thus we ignore the actual variation in ψ in regions of shock motion. This allows us to account for shock motions provided they remain small, which will generally be the case if $\varepsilon\tau^{-2/3} = o(1)$.

3. DISCRETIZATIONS OF THE GOVERNING EQUATIONS

An effective way to discretize Equation (7) is to use the alternating direction implicit (ADI) scheme introduced by Ballhaus and Steger [5] and subsequently refined by Ballhaus and Goorjian [6]. This method solves the governing equations in two steps. For simplicity, we discretize Equation (7) in the form

$$-2kM_\infty^2\psi_{xt} + (A\psi_x)_x + \psi_{yy} = 0,$$

where

$$A = \left[1-M_\infty^2 - (\gamma+1)M_\infty^2\phi_x^o\right].$$

Note that A is a known function of x and y.

Along a constant y line, predicted values of ψ, denoted by ψ^+, are computed using the formula

$$\frac{2k}{\Delta t} M_\infty^2 \overleftarrow{\delta}_x(\psi_{ij}^+ - \psi_{ij}^n) = D_x f_{ij}^+ + \delta_{yy}\psi_{ij}^n,$$

where

$$f_{ij} = A_{ij}\delta_x\psi_{ij},$$

and

$$D_x f_{ij} = \frac{2}{x_{i+1}-x_{i-1}} \cdot$$

$$[(1-\epsilon_i)(f_{i+1/2,j}-f_{i-1/2,j})+\epsilon_{i-1}(f_{i-1/2,j}-f_{i-3/2,j})],$$

with

$$\epsilon_i = \begin{cases} 0 \text{ if } A_{ij} > 0 \text{ (subsonic)} \\ 1 \text{ if } A_{ij} < 0 \text{ (supersonic)}, \end{cases}$$

and $\overleftarrow{\delta}_x$, δ_x, δ_{yy} are the backward-, central-, and second-central difference operators. This discretization provides the algebraic equations

$$[e,-a-b-d-e,a+b+c+d,-c] \begin{bmatrix} \psi_{i-2,j} \\ \psi_{i-1,j} \\ \psi_{ij} \\ \psi_{i+1,j} \end{bmatrix}^+ = [-a,a] \begin{bmatrix} \psi_{i-1,j}^n \\ \psi_{ij}^n \end{bmatrix} + \delta_{yy}\psi_{ij}^n \qquad (12)$$

where

$$a = \frac{2kM_\infty^2}{\Delta t \Delta x_i},$$

$$b = \frac{2(1-\epsilon_i)}{\Delta x_{i+1}+\Delta x_i} \frac{A_{i-1/2,j}}{\Delta x_i},$$

$$c = \frac{2(1-\epsilon_i)}{\Delta x_{i+1}+\Delta x_i} \frac{A_{i+1/2,j}}{\Delta x_{i+1}}$$

$$d = \frac{2\epsilon_{i-1}}{\Delta x_{i+1}+\Delta x_i} \frac{A_{i-1/2,j}}{\Delta x_i},$$

$$e = \frac{2\epsilon_{i-1}}{\Delta x_{i+1}+\Delta x_i} \frac{A_{i-2/3,j}}{\Delta x_{i-1}},$$

and

$$\Delta x_i = x_i - x_{i-1}.$$

Here the type-dependent upwind difference scheme of Murman and Cole is adopted to discretize the term $(A\psi_x)_x$ through the switching function ϵ_i. This scheme reduces to a central-difference scheme if the flow is subsonic, $A_{ij} > 0$, and to a backward-difference scheme if the flow is supersonic, $A_{ij} < 0$; in both cases, the matrix Equation (12) remains diagonally dominant.

Across the shock where A_{ij} is positive but $A_{i-1,j}$ is negative, the jump condition is implemented by setting d and e to zero and adding $(a+b)[\![\psi_{ij}^+]\!]$ to the right-hand side of Equation (12); in this calculation

$$[\![\psi_{ij}^+]\!] = -\frac{[\![A_{ij}]\!]\Delta t}{2kM_\infty^2} \tilde{\psi}_x^n(x_s^o, y^o) + [\![\psi_{ij}^n]\!],$$

and (13)

$$\tilde{\psi}_x^n = \frac{1}{2}\left(\frac{\psi_{i,js}^n - \psi_{i-1,js}^n - [\![\psi_{i,js}^n]\!]}{\Delta x_i} + \frac{\psi_{i-1,js}^n - \psi_{i,js}^n}{\Delta x_{i-1}}\right).$$

Here js represents the location y^o where the shock speed is computed, normally taken to be zero.

With the values of ψ^+ determined, the new values of ψ at the subsequent time level ψ^{n+1} are calculated using

$$\frac{2kM_\infty^2}{\Delta t}\delta_x(\psi_{ij}^{n+1} - \psi_{ij}^+) = \frac{1}{2}(\delta_{yy}\psi_{ij}^{n+1} - \delta_{yy}\psi_{ij}^n)$$

or the algebraic equation

$$[-\tilde{a},\tilde{a}+\tilde{b}+\tilde{c},-\tilde{b}]\begin{bmatrix}\psi_{i,j-1}\\ \psi_{ij}\\ \psi_{i,j+1}\end{bmatrix}^{n+1}$$

$$= \tilde{c}(\psi^{+}_{ij} - \psi^{+}_{i-1,j} + \psi^{n+1}_{i-1,j}) - \frac{1}{2}\,\delta_{yy}\psi^{n}_{ij}. \qquad (14)$$

Here

$$\tilde{a} = \frac{1}{(\Delta y_{i+1} + \Delta y_i)\Delta y_i},$$

$$\tilde{b} = \frac{1}{(\Delta y_{i+1} + \Delta y_i)\Delta y_{i+1}},$$

$$\tilde{c} = \frac{2kM_\infty^2}{\Delta t \Delta x_i},$$

$$\delta_{yy}\psi^{n}_{ij} = [\tilde{a},-(\tilde{a}+\tilde{b}),\tilde{b}]\begin{bmatrix}\psi_{i,j-1}\\ \psi_{ij}\\ \psi_{i,j+1}\end{bmatrix}^{n},$$

and

$$\Delta y_i = y_i - y_{i-1}.$$

Again, across the shock location x_s^o the jump of ψ, or the term

$$\tilde{c}([\![\psi]\!]^{n+1} - [\![\psi]\!]^{+}) = \tilde{c}\,\frac{[\![A_{ij}]\!]\Delta t}{2kM_\infty}\,\psi^{n}_{x}(x_s^o, y^o) \qquad (15)$$

is added to the right-hand side of Equation (14).

The full procedure is, effectively,

$$\frac{2kM_\infty^2}{\Delta t} \overset{+}{\delta}_x(\psi^{n+1}_{i,j} - \psi^{n}_{ij})$$

$$= D_x f^{+}_{ij} + \frac{1}{2}\,\delta_{yy}(\psi^{n+1}_{ij} + \psi^{n}_{ij}) \qquad (16)$$

with the jump condition implemented through the form of Equations (13) and (15). It can be shown through a von Neumann analysis that, shock motion aside, this scheme is unconditionally stable, that is, there is no restriction on the time step Δt. However, for mixed flow, the integration of Equation (11), or its equivalent Equation (13), for the shock motion restricts the use of large time steps for both accuracy and stability.

3.1. Boundary Conditions

A typical computational domain is shown in Fig. 2. On the slit representing the airfoil, the boundary condition (6a) becomes

$$\frac{\psi^{n+1}_{i,j+1} - \psi^{n+1}_{i,j}}{\Delta y_{j+1}} = Y^u_x + kY^u_t, \quad 0 < x_i \leq 1$$

and in the wake Equation (6) is approximated by using characteristics, i.e.,

$$\left[\left[\psi^{n+1}_{ij}\right]\right] = \begin{cases} (1-r)\left[\left[\psi^{n}_{ij}\right]\right] + r\left[\left[\psi^{n}_{i-1,j}\right]\right], & r = \frac{\Delta t}{k\Delta x} < 1 \\ (1 - \frac{1}{r})\left[\left[\psi^{n+1}_{i-1,j}\right]\right] + \frac{1}{r}\left[\left[\psi^{n}_{i-1,j}\right]\right], & r > 1 \end{cases}$$

which is unconditionally stable and superior to the implicit central-difference scheme or the upwind-backward difference scheme often employed.

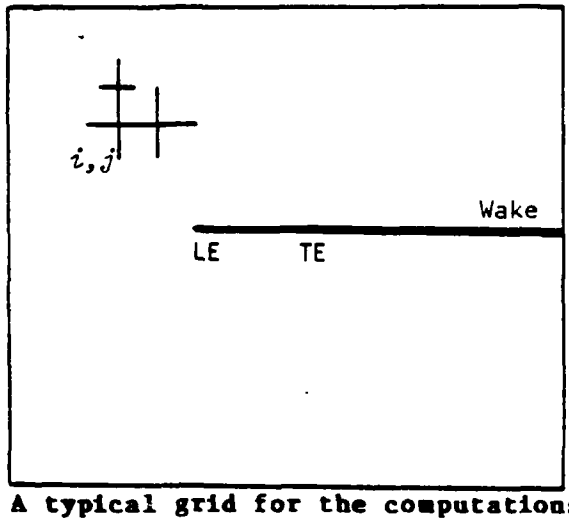

Figure 2. A typical grid for the computations described in this chapter.

4. PRESSURE INPUT STEADY STATE

The solution to Equation (7b) depends critically on the steady state ϕ^o_x, that is, on the local perturbed pressure field. This is especially true when there is an embedded supersonic zone where ϕ^o_x exceeds its sonic value $(1-M_\infty^2)/(\gamma+1)M_\infty^2$. In this case, an accurate prediction of the steady flow field is essential. However, if the flow field is everywhere subsonic, i.e., $\phi^o_x < (1-M_\infty^2)/(\gamma+1)M_\infty^2$, this dependency is not as important since there is no change of equation type.

To obtain an accurate steady flow field, particularly in the transonic regime, the small disturbance theory often is inadequate due to its local failure at the leading edge and, in some cases, to the limitation on shock strength. Although this problem can be circumvented by using numerical codes based on the full potential equations, or even better, the Euler equations, the cost of using such codes in engineering applications, such as the prediction of flutter boundaries, is prohibitively high. The grid systems that are essential for such calculations are unnecessary for the unsteady flow and may even be harmful due to stringent time step requirements associated with locally refined meshes. More importantly, viscous effects have been ignored. Following Fung and Chung [4], we develop a method that allows the algorithm developed here to be applied to an airfoil for which we have an accurate steady-state pressure distribution. Thus, this algorithm can be implemented to determine the unsteady response of an airfoil whose steady pressure distribution is known. In this way, at least steady viscous effects are accounted for. As we shall discuss later, it is much easier to get accurate steady-state transonic results than unsteady ones because experimental flows are easily contaminated by the reflections of unsteady disturbances from wind tunnel walls.

Since an accurate steady-state pressure field is desired, we find the small perturbation flow field that corresponds to a pressure distribution provided from wind tunnel measurements or accurate numerical computations. This is referred to as an inverse design problem: find an airfoil that has a given pressure distribution.

In the inverse problem, since pressure is given, the values of ϕ^o on the slit representing the airfoil are known, up to an arbitrary constant c', from integrating ϕ^o_x. To determine this constant c', a closure condition is required. In small disturbance theory, since ϕ_y is equivalent to the body slope, a closed airfoil requires that

$$\int_0^1 [\phi^o_y(x,0^+) - \phi^o_y(x,0^-)]dx = 0.$$

Although the numerical computations cannot normally satisfy this condition exactly, it provides a means of determining the constant c'.

An iterative process is used to solve Equation (1) for the steady state ϕ^o. The value $\Delta c'$ found from

$$\frac{\Delta c'}{\Delta y} = \alpha \{ \int_0^1 [\phi^o_y(x,0^+) - \phi^o_y(x,0^-)]dx - \kappa \} \qquad (17)$$

is added to every unsteady value ϕ^n_{ij}, the nth iterate of ϕ at

$$\varphi_{ij}^{n+1} = \varphi_{ij}^{n} + \Delta c'.$$

until a steady state is reached. The relaxation factor in Equation (18) helps converge the calculations to their steady state; the small parameter κ is added to yield a smooth body slope distribution. Detailed descriptions of this procedure can be found in Fung and Chung [4].

Once a steady flow field is obtained, the unsteady response is calculated using the algorithm described earlier or the LTRAN2 code developed in Ref. [6] with the body slopes determined by the inverse procedure.

5. INDICIAL RESPONSE METHOD

A major advantage of time linearization is the possibility of using superposition; that is, adding solutions that are independent to form a composite solution in time. Basically, if the system used is linear in time, including the governing equations and the associated boundary conditions, and if $\phi_1(t)$ and $\phi_2(t)$ are solutions, then the composite $\alpha_1\phi_1 + \alpha_2\phi_2$ is also a solution. For example, if the change in lift coefficient of an airfoil as a function of time for a step change in angle of attack is $C_{\ell\alpha}(t)$, then the lift coefficient, $C_\ell(t)$, for a variation, $\alpha(t)$, in angle of attack is

$$C_\ell(t) = C_\ell(t)\alpha(o) - \int_o^t C_{\ell\alpha}(t') \frac{d\alpha(t-t')}{dt'}\, dt', \qquad (18)$$

a direct application of the Duhamel integral. Through linearization, the system of Equations (5), (6a), and (6b) is linear and its dependence on k can be removed by simply scaling k. Consequently, sinusoidal variations of any reduced frequency k are obtainable from the indicial response of a step change using Equation (18).

6. NUMERICAL EXAMPLES

To demonstrate the merits of the time linearized method, we choose a set of measurements for a NACA 64A010 airfoil at $M_\infty = 0.8$ from the well documented experiments of Davis and Malcolm [7]. In these experiments, the airfoil was pitching at an angle 1.0° sinusoidally over a range of reduced frequencies. Figure 3 shows the experimental steady pressure distribution on this airfoil. This pressure distribution was used as input to the inverse algorithm IAF2 [4] that provides the steady flow field used later in UTFC, the algorithm based on Equation (16). Because there were nineteen measured pressure values from these experiments, a 100 x 80 grid with 23 mesh points on the airfoil was chosen.

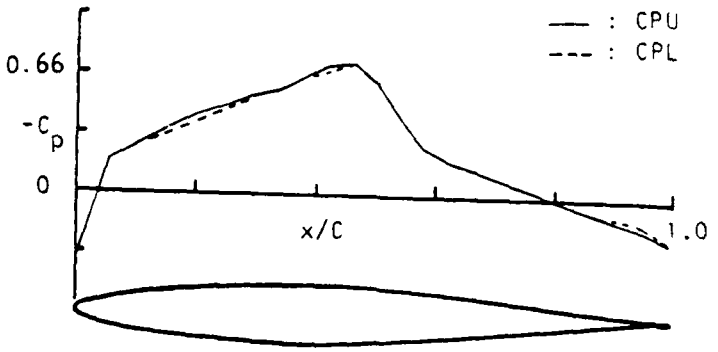

Figure 3. Upper and lower steady surface pressure from the experiments of Ref. 7 for a NACA 64A010 airfoil, M_∞ = 0.8.

Figure 4 compares the lift and moment coefficients obtained from UTFC with those from the experiments and from LTRAN2-HI, a nonlinear code based on Equation (7a). Overall agreement between the measured and computed values exists. Note also how well the results from UTFC agree with those from LTRAN2-HI, verifying that time linearization provides an adequate approximation for sufficiently small ε. Furthermore, it seems that the magnitudes of the moment coefficient from UTFC are closer to the experimental values than those from LTRAN2, which is attributed to the better treatment of moving shock waves in the time-linearized theory when the amplitude of motion is small.

Compared to the magnitudes, which are in excellent agreement with the measured values, the phase angles are in only moderately good agreement. Numerical experiments discussed in the next section indicate that this discrepancy is due to wind tunnel interference.

It is worth mentioning that all the results from UTFC were obtained using 120 time steps per cycle, or 3° of circular oscillation per time step, for all frequencies and that no instability due to time step limitation was observed. However, it was reported by Hessenius and Goorjian [8] that in order to produce a stable solution at $k = 0.5$ using LTRAN2-HI, as many as 1440 time steps per cycle were necessary. As discussed in [9], this is attributed to the leading edge over-expansion, to unnecessary local mesh refinements, and/or to the shock over-shoot as a result of the Murman-Cole switching that may admit temporal expansion shocks; however Goorjian and van Buskirk [9], also reported

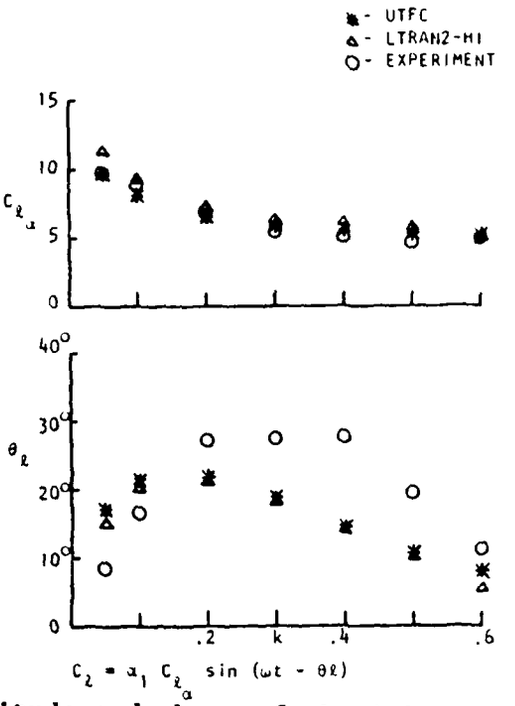

4a. Amplitude and phase of the lift coefficients.

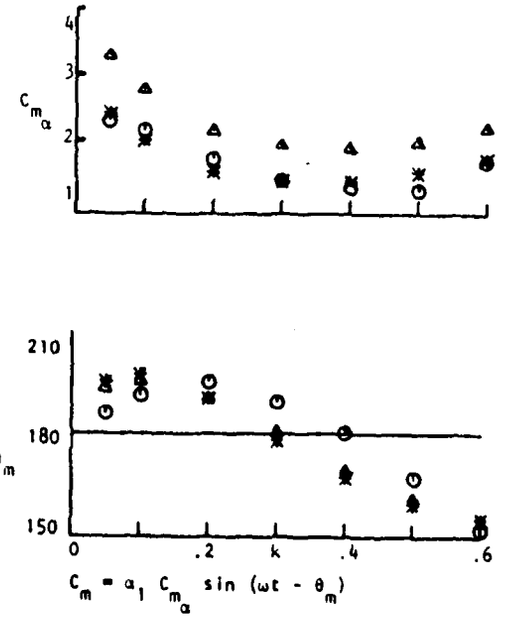

4b. Amplitude and phase of the moment coefficients.

Figure 4. Lift and leading edge moment coefficients vs reduced frequency for a pitching NACA 64A010 airfoil, $M_\infty = 0.8$.

that the monotone scheme of Engquist-Osher removes the nonlinear instability of over-expansion. This problem does not occur in the time-linearized formulation because the local Mach number, which determines the type of differencing in the Murman-Cole formulation, depends only on the steady-state values ϕ_x^0 and this is unaffected by the unsteady perturbations.

7. WIND TUNNEL WALL EFFECTS

The accuracy and reliability of wind tunnel experiments have been difficult to assess, particularly in the transonic regime. The presence of wind tunnel walls, which in practice are seldom farther than ten chords away from the testing airfoil, makes the simulation of free flight conditions difficult. Many attempts have been made to minimize wall interferences, including wall ventillation through slots as used in the Davis and Malcolm [7] experiments, the smart wind tunnel with adjustable wall porosity proposed by Sears [10], and the flexible wall method developed by Goodyer [11]. However, none of these methods were designed to eliminate or minimize unsteady wall interference.

Except for solid walls, where the boundary conditions are well defined, the general wall conditions in experiments do not lend themselves to analytical modeling, making quantitative comparisons between numerical and experimental results difficult, if not impossible. Figure 5 shows typical variations of the lift coefficient, C_ℓ, as a function of time, measured in chord length travelled, for an airfoil after a sudden change in incidence. Notice that after a lapse of about 100 chord lengths, the lift coefficient reaches 90% of its steady value - the solid curve computed using a grid whose boundaries are 87 chords away from the airfoil - indicating that the wind tunnel wall reflections did not have enough time to return to the airfoil. The values shown by the asterisks, obtained with boundary conditions satisfying Equation (4) posed at the grid boundary 13 chords away, agree very well with the solid curve, implying that Equation (4) is a good representation of the solution at that distance and that no significant wall interference is detected except, perhaps, some minor nonlinear effects.

Also shown in Figure 5 are the results (stars) obtained using the non-reflective boundary conditions of Engquist and Majda [12] and that using the constant pressure condition,

$$\phi_x = 0.$$

The non-reflective boundary condition,

$$(1-M_\infty^2)^{1/2}\,\psi_x \pm \psi_y = 0, \text{ on } y = \pm y_{max},$$

stating that far away only one family of outgoing waves along the characteristics $dy/dx = \pm 1/(1-M_\infty^2)^{1/2}$, achieves about 90% of the steady-state lift and gives a substantial improvement over the constant pressure condition, which causes a 30% reduction in magnitude of the lift coefficient and a shortened characteristic time of only 40 chords.

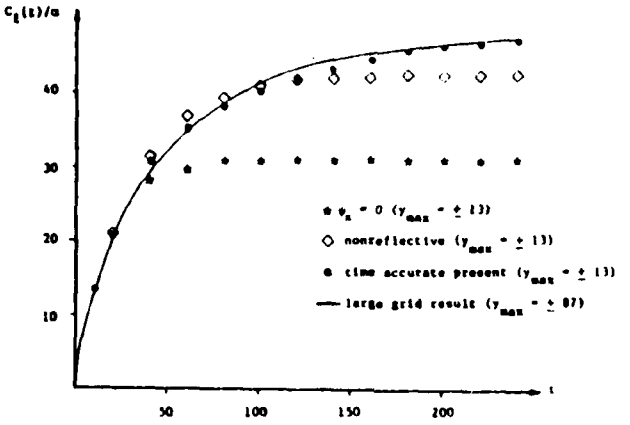

Figure 5. Indicial pitch response for an NACA 64A006 at $M_\infty = 0.88$.

It is observed that in these numerical experiments the lift coefficient reaches a new steady value that depends on the condition at the far-field boundaries through a process describable by the simple model

$$C_\ell(t) = C_\ell(\infty)(1-e^{-\lambda t}), \tag{20}$$

where $1/\lambda$ denotes a characteristic time. Substituting Equation (20) into Equation (18) and assuming harmonic pitching motions, $\alpha(t) = \sin kt$, the unsteady lift coefficient is then

$$C_\ell(t, k) = \frac{C_\ell(\infty)}{\left[1 + (\frac{k}{\lambda})^2\right]^{1/2}} \sin(kt - \tan^{-1}\frac{k}{\lambda}) \tag{22}$$

This result shows that for low reduced frequencies, the magnitude and the phase depend on the parameter (k/λ). For typical transonic flows over an airfoil, λ is small and decreases rapidly with Mach number. Due to wall confinement in a typical wind tunnel experiment, the steady value $C_\ell(\infty)$ would be smaller and the characteristic time $1/\lambda$ would also be smaller than those measured in unbounded flow. Hence the magnitude of the unsteady lift coefficient measured in a wind tunnel would be smaller; its decrease with k not as rapid due to the larger λ. Also, the phase lag increase with

k would not be as rapid. These observations are consistent with the results shown in Figure 4. For high reduced frequencies, the effects of wall boundary condition are poorly understood. In the case of a solid wall, resonance is known to occur, but most tunnel walls are ventilated, mitigating the effects of resonance.

Figure 6 compares the same set of experimental values in Figure 4 with that of a time linearized calculation using the steady pressure as measured in the experiment as input and with the solid wall condition, $\phi_y = 0$, prescribed at the grid boundary 7.2 chords away from the airfoil. At the frequencies $k = 0.125$ and $k = 0.325$, the resonance condition as indicated by suddent drops of magnitude and phase seems to occur. Figure 7 shows similar comparisons, but with the non-reflective boundary condition described earlier applied at 7.2 chords. For moderate reduced frequencies, $k \geq 0.2$, the computed values (triangles) for a finite boundary as close as 7.2 chords away are the same as those for an unbounded region, but for low reduced frequncies, these values are closer to the experimental ones, indicating the presence of wall interference. Figure 8 shows again similar comparisons with the linear asymptotic far-field condition, Equation (4) prescribed at the same distance, but with the phase of $\Gamma(t)$ arbitrarily adjusted to compensate for the time that might have taken the signal to reach the boundary. Surprisingly, these values, especially the phase angles, coincide with the experimental results, indicating the importance of wall interference and that part of the interference is due to nonlinear effects not accounted for in a strict application of Equation (4).

Although a general description of wind tunnel wall interference is still lacking, these numerical experiments have indeed demonstrated the seriousness of the problem. More detailed discussion of wall interference, including three-dimensional effects, can be found in Przybytkowski [13].

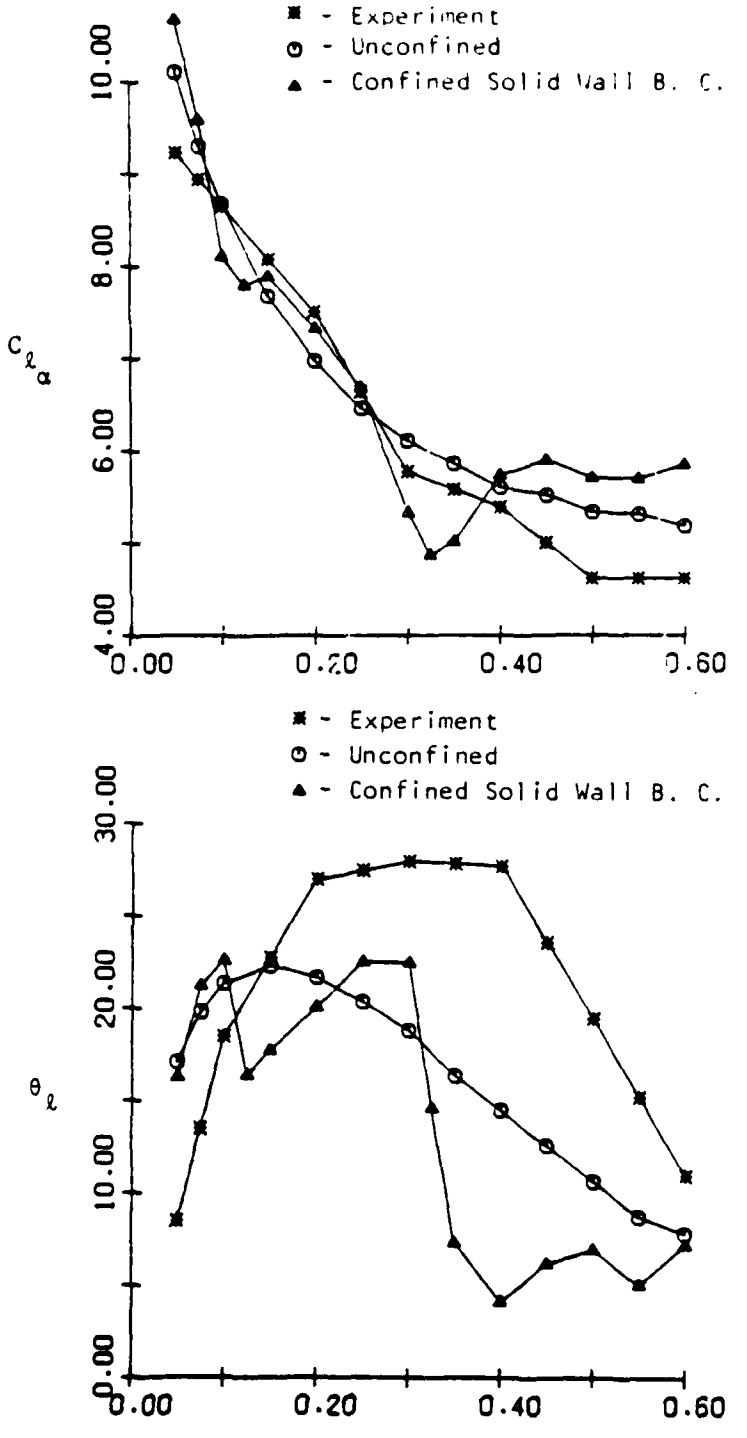

Figure 6. Comparisons of the lift coefficients using the solid wall boundary condition at a distance, $y_{max} = 7.2$.

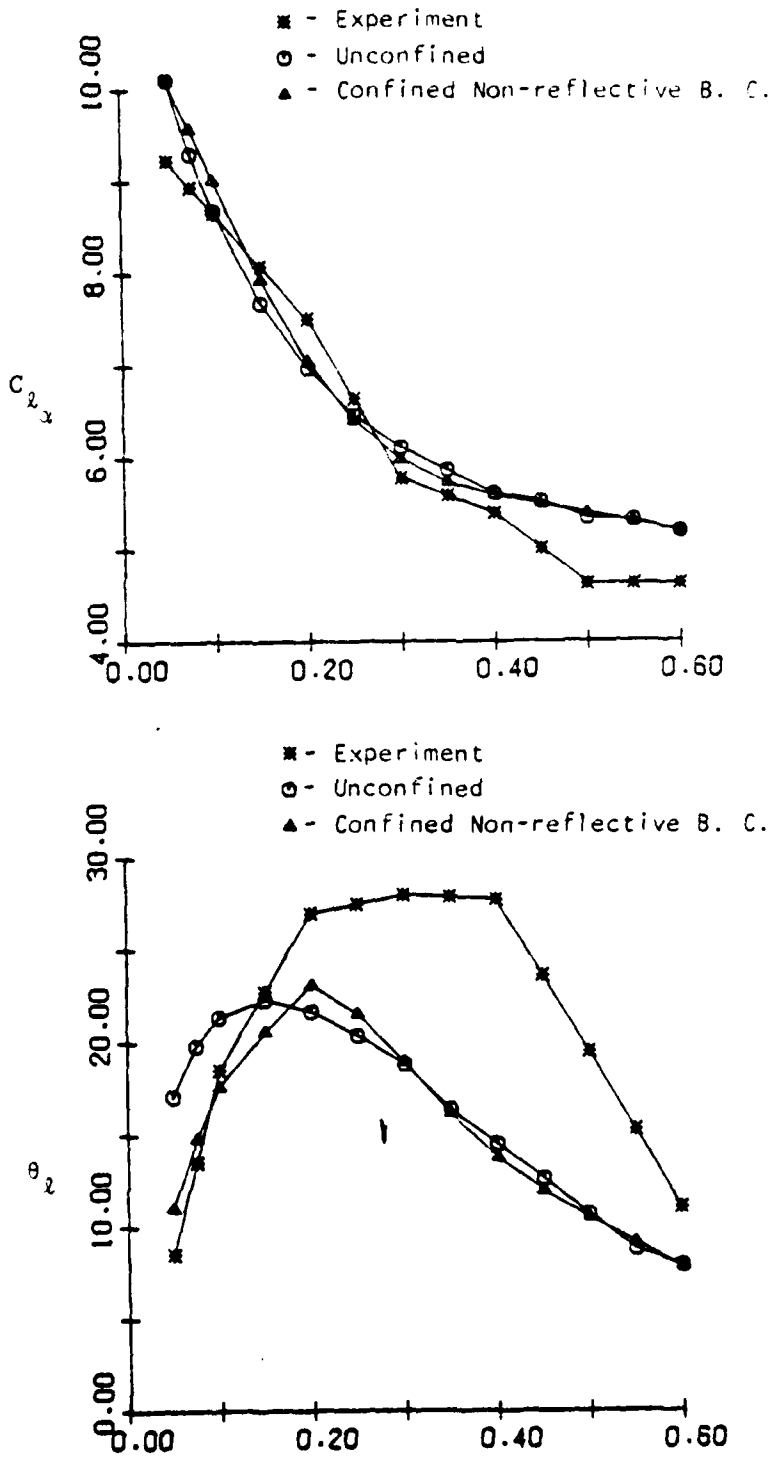

Figure 7. Comparison of the lift coefficients using the non-reflective boundary condition at a distance, $y_{max} = 7.2$.

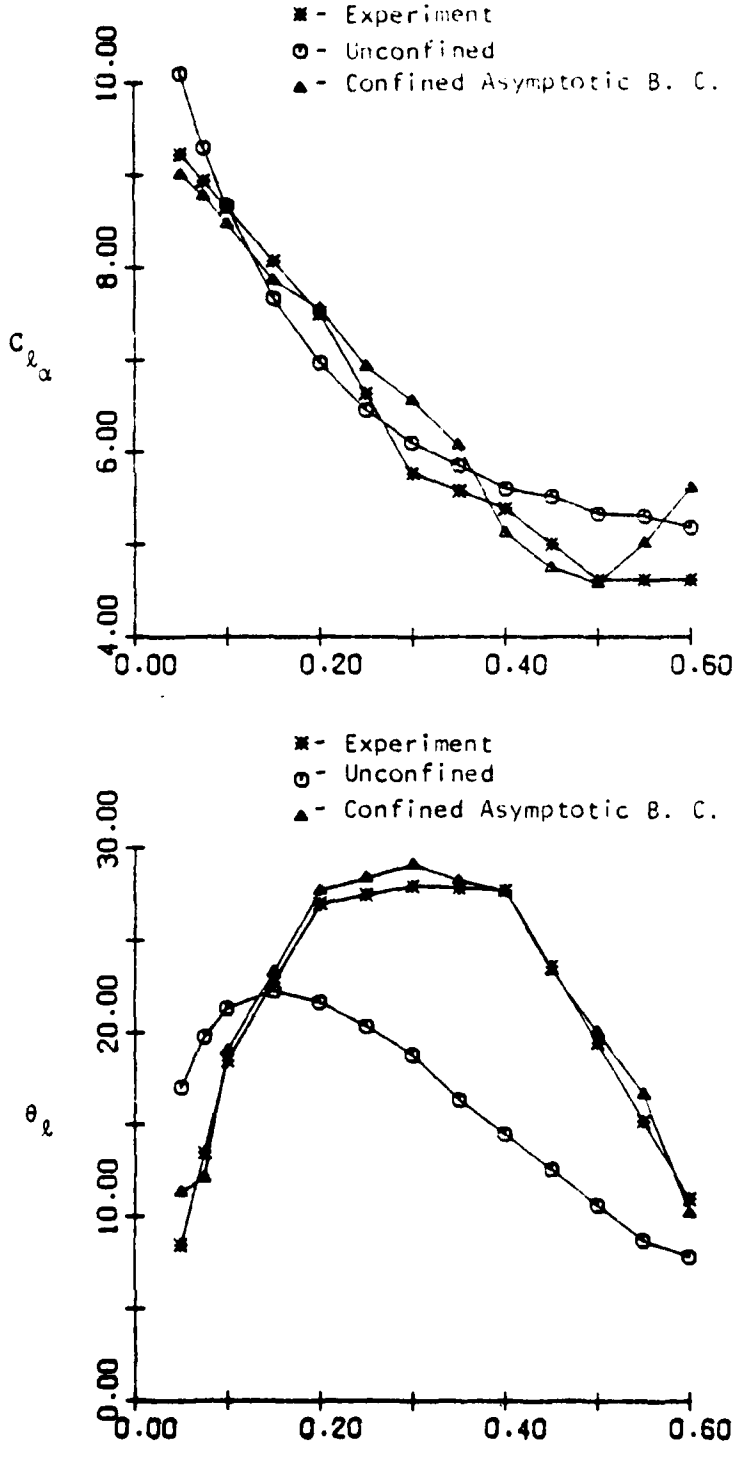

Figure 8. Comparisons of the lift coefficients using asymptotic boundary condition at a distance, y_{max} = 7.2.

CONCLUSION

We have shown in this chapter that for small unsteady disturbances, the time-linearization technique provides accurate descriptions of the flow fields despite its simplicity. It allows the decoupling of the unsteady flow field from the steady flow field, which could be obtained more efficiently and accurately by other means, including direct experimental measurements. The extension of this procedure to three-dimensional flow fields using strip theory for high aspect ratio wings is straightforward, the savings are substantial and the success warranted.

The numerical examples discussed here demonstrate the importance of wall interference in unsteady transonic wind tunnel measurements, which deserves a better understanding.

ACKNOWLEDGMENTS

This work was supported by the AFOSR through Grant No. 896875 and by NASA through Grant No. NGT-03-002-800.

REFERENCES

1. LIN, C. C., T. REISSNER, H. S. TSIEN - On Two-Dimensional Non-Steady Motion of a Slender Body in a Compressible Fluid. J. Math Phys., Vol. 3, pp.220-31, 1948.

2. FUNG, K.-Y. - Far Field Boundary Conditions for Unsteady Transonic Flows. AIAA Journal, Vol. 19, pp. 180-83, 1981.

3. YU, N. J., SEEBASS, A. R., BALLHAUS, W. F. - Implicit Shock-Fitting Scheme for Unsteady Transonic Flow Computations. AIAA Journal, Vol. 16, pp. 673-78, 1978.

4. FUNG, K.-Y. and CHUNG, A. - Computation of Unsteady Transonic Aerodynamic Responses Using a Prescribed Input Steady State Pressure Distribution, AIAA-82-0956, AIAA/ASME 3rd Joint Thermophysics, Fluids, Plasma and Heat Transfer Conference, St. Louis, Missouri, 1982, to appear in AIAA Journal.

5. BALLHAUS, W. F., STEGER, J. L. - Implicit Approximate-Factorization of Unsteady Transonic Flows by the Indicial Method. AIAA Journal, Vol 16, pp.117-24, 1975.

6. BALLHAUS, W. F., GOORJIAN, P. M. - Implicit Finite-Difference Computations of Unsteady Transonic Flows About Airfoils. AIAA Journal, Vol. 15, pp.1728-35, 1977.

7. DAVIS, S. S. and MALCOLM, G. N., Experimental Unsteady Aero-Dynamics of Conventional and Supercritical Airfoils. NASA TM-81221, 1980.

8. HESSENIUS, K. A. and GOORJIAN, P. M. - Validation of LTRAN2-HI by Comparison with Unsteady Transonic Experiment. AIAA Journal, Vol. 20, pp. 731-32, and NASA TM-81037, 1982.

9. GOORJIAN, P. M. and Van Buskirk, R. - Implicit Calculations of Transonic Flows Using Monotone Methods. AIAA 19th Aerospace Sciences Meeting St. Louis, Missouri, 1981.

10. SEARS, W. R. - A Note on Adaptive-Wall Wind Tunnels. Journal of Applied Mathematics and Physics, Vol. 28, pp. 915-27, 1977.

11. GOODYER, M. J. - The Self-Streaming Wind Tunnel, NASA TMX-72699, 1975.

12. ENGQUIST, B. and MAJDA, A. - Numerical Radiation Boundary Conditions for Unsteady Transonic Flows. Journal of Computational Physics, Vol. 40, pp. 91-103, 1981.

13. PRZYBYTKOWSKI, S. M. - Effect of Wall Interference in Unsteady Transonic Flows. Ph.D. Thesis, University of Arizona, 1983.

APPENDIX D

Vorticity at the Shock Foot in Inviscid Flow

K.-Y. Fung

Reprinted from
AIAA Journal
Volume 21, Number 6, June 1983, Page 915

AMERICAN INSTITUTE OF AERONAUTICS AND ASTRONAUTICS • 1290 AVENUE OF THE AMERICAS • NEW YORK, NEW YORK, N.Y. 10104

Vorticity at the Shock Foot in Inviscid Flow

K.-Y. Fung*
University of Arizona, Tucson, Arizona

Introduction

IT is characteristic of transonic flows to have a shock or shocks embedded in the flowfield. The flow immediately behind the shock is related to the flow ahead of it by the Rankine-Hugoniot conditions and is a function of the shock shape. If the shock is normal to the body surface, the flow behind the shock will be subsonic and its shape will, in general, not be known a priori. The shock shape must be determined in conjunction with the local flowfield.

Although inviscid transonic flow past a body can be computed routinely using numerical methods developed in the last decade, the shock region has always been the most erroneous part of the solution. Often the potential approximation is made, and this is inconsistent with the conservation of normal momentum across the shock. Also, only the weak form of the governing equation is satisfied to an order normally so restricted by numerical stability that the actual shock is smeared over several grid points. As the shock gets stronger, entropy and vorticity production behind the shock can no longer be ignored and potential theory fails. These effects, added to the already complex flowfield, makes the construction of a proper numerical scheme a difficult task.

In this Note we study the flowfield immediately downstream of a shock at its root where the shock meets a smooth convex surface. Lin and Rubinov[1] first noted that a singularity occurs at the shock root. They also argued that the shock shape at the root must be of the form

$$\xi = k\eta^{3/2}$$

where ξ, η are coordinates of the shock measured along and normal to the body, respectively. Zierep[2] also found the same shock shape but was unable to determine the constant k for a convex body. Later Gadd[3] pointed out that the flow behind and at the shock root, determined by the Rankine-Hugoniot conditions, experiences a discontinuity in curvature in order to conform to the body. Such a flow is known to have a multivalued normal pressure gradient and a streamwise pressure gradient that is logarithmically singular.

We shall determine the vorticity behind the curved shock at this singular point and discuss to what extent the flowfield is affected by this vorticity.

Shock-Induced Vorticity

It is well known that the vorticity behind a shock can be computed by applying Crocco's theorem, i.e.,

$$\zeta_2 = -\frac{1}{q_2 \sin(\sigma-\alpha)}\left[\frac{1}{2}\frac{dq_2^2}{d\ell} + \frac{1}{\rho_2}\frac{dp_2}{d\ell}\right] \tag{1}$$

where subscript 2 denotes quantities evaluated after the shock, ζ is the vorticity induced by the shock, q the flow speed, ρ the density, p the pressure, ℓ the distance along the shock, σ the shock angle measured relative to the upstream flow, and α the flow deflection angle after the shock (Fig. 1).

The Rankine-Hugoniot conditions require that the post-shock quantities be related to preshock quantities as follows:

$$q_2^2 = q_1^2[1-(1-\epsilon^2)\sin^2\sigma]$$

$$p_2 = p_1 + \rho_1 q_1^2(1-\epsilon)\sin^2\sigma$$

$$\epsilon = \frac{\rho_1}{\rho_2} = \frac{\gamma-1}{\gamma+1} + \frac{2}{(\gamma+1)M_1^2\sin^2\sigma} \tag{2}$$

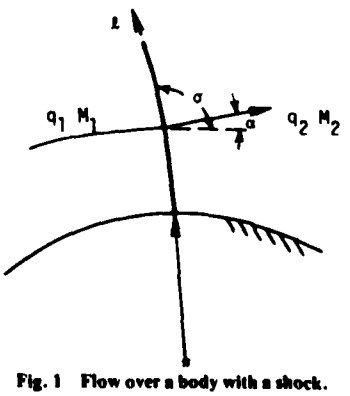

Fig. 1 Flow over a body with a shock.

Received July 1, 1982. This paper is declared a work of the U.S. Government and therefore is in the public domain.

*Assistant Professor. Member AIAA.

Dedicated to Professor William R. Sears in celebration of his 70th birthday, with the author's admiration.

where the subscript 1 denotes quantities ahead of the shock, γ is the ratio of the specific heats, and M is the Mach number. After substituting Eq. (2) into Eq. (1), we see that the vorticity equation becomes

$$\zeta_2 = -\frac{(1-\epsilon)q_1}{\epsilon\sin\sigma}\left\{[\epsilon(M_1^2-1)\sin^2\sigma-\cos\sigma]\frac{1}{\rho_1 q_1^2}\frac{dp_1}{d\ell}\right.$$

$$\left.-(1-\epsilon)\sin\sigma\cos\sigma\frac{d\sigma}{d\ell}\right\} \tag{3}$$

At the shock root where the shock is normal this formula can be further simplified to

$$\zeta_2 = -\frac{(1-\epsilon)q_1}{\epsilon}\left[\frac{\epsilon(M_1^2-1)}{R}-(1-\epsilon)\cos\sigma\frac{d\sigma}{d\ell}\right] \tag{4}$$

where R is the radius of curvature of the body at the shock root. We note that the last term on the right-hand side of Eq. (4) cannot be evaluated immediately but $\cos\sigma(d\sigma/d\ell)$ must be negative since $\sin\sigma$ attains its maximum at the root with $\sigma=\pi/2$. We thus conclude that the vorticity is clockwise or negative, and is a second-order quantity proportional to $(1-\epsilon)^2$ since, from Eq. (2),

$$1-\epsilon=\frac{2(M_1^2\sin^2\sigma-1)}{(\gamma+1)M_1^2\sin^2\sigma} \tag{5}$$

In order to evaluate the vorticity, the shock shape $\sigma(\ell)$ must be found. We note here that the potential approximation is only valid to second order at the shock root unless $1/R=0(1-\epsilon)$, i.e., unless the slender body approximation is made.

Flow Behind the Shock

The inviscid subsonic flow after the shock would be rotational in general and therefore is governed by the Euler equations. The continuity equation, written in intrinsic coordinates s and n, along and normal to flow, is

$$\frac{\partial\rho q}{\partial s}+\rho q\frac{\partial\theta}{\partial n}=0 \tag{6}$$

The vorticity equation by definition is

$$\zeta=q\frac{\partial\theta}{\partial s}-\frac{\partial q}{\partial n} \tag{7}$$

where θ is the flow angle measured with a fixed reference frame.

If one defines an intrinsic stream function Ψ as

$$\Psi_n=\ell n\rho q \quad \text{and} \quad \Psi_s=-\theta$$

then, Eq. (6) is automatically satisfied and Eq. (7) becomes

$$(1-M^2)\Psi_{ss}+\Psi_{nn}=-\frac{[1+(\gamma-1)M^2]}{q}\zeta \tag{8}$$

This equation can be solved for Ψ with given ζ as in Eq. (4) by specifying Ψ at $n=0$; Ψ_s and Ψ_n at the shock boundary $\ell(s,n)$ with Ψ_s and Ψ_n being finite at downstream infinity. The requirement that this elliptic system is not being over-specified thus determines the shock.

In general, Eq. (8) can only be solved by numerical means; however, a local expansion, making use of the fact that the vorticity is only a second-order quantity as mentioned earlier, can be very informative in understanding the flow behind a shock.

Vorticity at the Shock Root

Since vorticity is shown to be of the order of $(1-\epsilon)^2$, a formal expansion, e.g., $\Psi=\Psi^0+\delta\Psi^1+\ldots$ in a small parameter $\delta=\delta(1-\epsilon)$, yields the lowest order equation for Ψ valid at the vicinity of the shock root as follows

$$(1-M_2^2)\Psi^0_{ss}+\Psi^0_{nn}=0 \tag{9}$$

The solution of this equation subject to the stated boundary conditions was first given by Gadd[2] and later solved in a more formal manner by Oswatitsch and Zierep.[3] The shock shape they found, which is different from that predicted by Lin and Rubinov,[1] is normal to the body and has a logarithmic singularity in curvature at the body. The unknown quantity, $\cos\sigma(d\sigma/d\ell)$, evaluated at the shock root is then zero.

We conclude that since vorticity is second order the flowfield behind the shock remains irrotational to the lowest order. The local curvature of shock at the shock root, despite being logarithmical-infinite, does not contribute to the vorticity. For slender bodies the shock curvature as well as the body curvature are $0(1-\epsilon)$. Thus our result for vorticity reduces to the usual small disturbance result of $(1-\epsilon)^3$.

Since all the higher order equations are of Poisson-type with homogeneous boundary conditions, their solutions should be regular and have no more singular contribution to the shock curvature at the root than the lowest order logarithmic one. We then obtain the equation for vorticity at the root as

$$\zeta_2=-\frac{(1-\epsilon)q_1}{R}(M_1^2-1) \tag{10}$$

where

$$\epsilon=\frac{\gamma-1}{\gamma+1}+\frac{2}{(\gamma+1)M_1^2}$$

in terms of known quantities q_1 and M_1, upstream of the shock and the body curvature $1/R$.

Conclusion

We have shown that vorticity behind the shock is of the order of $(1-\epsilon)^2$ even at the shock root where the curvature of the shock is infinite, and have obtained a formula for this vorticity valid at the root in terms of upstream quantities only. This formula can be used in the construction of an accurate numerical scheme for Eq. (8).

Acknowledgment

This research was supported by the ONR through Grant No. N00014-76-C-0182, P00006 and the AFOSR through Grant No. 81-0107.

References

[1] Lin, C. C. and Rubinov, S. I., "On the Flow Behind Curved Shocks," *Journal of Mathematical Physics*, Vol. 27, 1948, pp. 105-129.

[2] Zierep, J., "Der senkrechte Verdichtungsstoss am gekrümmten Profile," *Zeitschrift fuer Angewandte Mathematik und Physik*, Vol. 9b, 1958, p. 764.

[3] Gadd, G. E., "The Possibility of Normal Shock Waves on a Body with Convex Surfaces in Inviscid Transonic Flow," Kurze Mitteilungen-Brief Reports, *ZAMP*, Vol. XI, 1960, pp. 51-58.

[4] Oswatitsch, K. and Zierep, J., "Das Problan des senkrechten Stosses an einer gekrummten Wand," *ZAMM*, Vol. 40, 1960, p. 143.

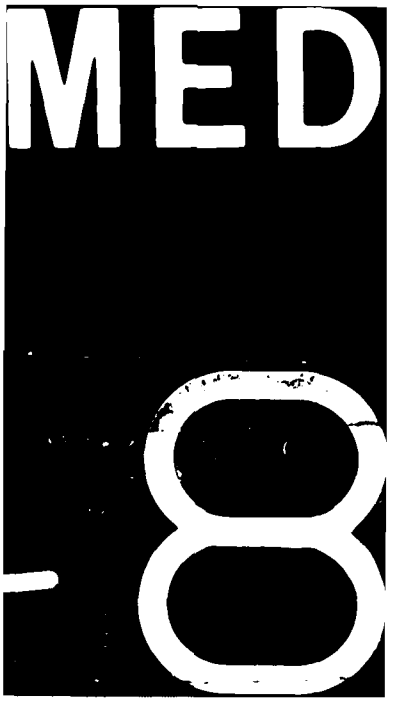
MED
8